WHIRL FLUTTER SUPPRESSION WITH PASSIVE DYNAMIC VIBRATION ABSORBERS

Hande Erturan*
Turkish Aerospace Industries
Istanbul Technical University
Istanbul, Turkey

Ali Tatar
Istanbul Technical University
Istanbul, Turkey

ABSTRACT

Aeroelastic phenomena have significantly influenced the design of aircraft and engines throughout the history of aviation. A prominent example of such a challenge is whirl flutter—an aeroelastic instability that occurs due to the interaction between aerodynamic forces and gyroscopic effects in rotating parts like propellers and fans. This form of instability, rooted in the inherent dynamics of the system, can result in severe and potentially catastrophic outcomes. In recent years, whirl flutter has gained growing attention as a critical concern, particularly with the rise of advanced tiltrotor aircraft, distributed propulsion systems, and other cutting-edge rotorcraft technologies. This study aims to expand the speed range by increasing the whirl flutter speed in vertical propeller systems by adding a passive dynamic vibration absorber to the system. In the newly created dynamic system, the modal damping and frequency behavior of the system is examined by using the standard eigenvalue problem solution. In addition, a baseline system was used and parameters are created to see the passive dynamic vibration absorber effects fully. Numerical simulation results indicate that this approach can effectively enhance the aircraft's critical whirl flutter speed. The extent of this improvement is strongly influenced by key parameters, particularly the mass ratio between the dynamic vibration absorber and the propeller, as well as the frequency ratio between their respective vibration modes. Optimizing these ratios allows the dynamic vibration absorber to efficiently counteract the destabilizing aeroelastic forces, thereby raising the onset speed of whirl flutter and improving the overall stability margin of the system.

NOTATION

*

Symbols

a Distance between propeller hub and center of gravity, m

A_1, A_2, A_3 Aerodynamic coefficients of propeller

c_b Chord length of propeller blades, m

$c_{l,\alpha}$ Lift slope of propeller blades, rad^{-1}

C_{θ_p}, C_{ψ_p} Structural damping of proprotor support, Nms rad^{-1}

C_{θ_a}, C_{ψ_a} Structural damping of absorber mass, Nms rad^{-1}

I_{na} Moment of inertia of the absorber mass, kg m^2

I_{np} Moment of inertia of the nacelle, kg m^2

I_x Moment of inertia of the rotor, kg m^2

K_a Aerodynamic coefficient of propeller

K_{θ_p}, K_{ψ_p} Structural stiffness of proprotor support, Nm rad^{-1}

K_{θ_a}, K_{ψ_a} Structural stiffness of absorber mass, Nm rad^{-1}

M_θ Applied moment in pitch direction, Nm

M_ψ Applied moment in yaw direction, Nm

N_b Number of blades

R Rotor Radius

V Velocity of the aircraft, m/s

β Frequency ratio

ε Mass ratio

ζ Damping ratio

θ_p, ψ_p Propeller pitch and yaw angle, rad

θ_a, ψ_a Absorber pitch and yaw angle, rad

μ Propeller advance ratio

ρ Air density, kg/m^3

Ω Angular velocity of the propellers, rad/s

ω Natural frequency, rad/s

*

Acronyms

DOF Degrees-of-freedom

INTRODUCTION

With the progression of aviation technology, the demand for more sophisticated and high-performance systems and structures has grown, giving rise to critical phenomena like aeroelasticity. Whirl flutter is a significant challenge, characterized as an aeroelastic instability caused by the interaction between aerodynamic forces and gyroscopic effects in rotating elements like propellers and fans (Ref. 1). This dynamic instability, driven by the system's inherent dynamics, can result in catastrophic structural failures and decrease the safety margin. Recently, the importance of whirl flutter has grown markedly, particularly with the advancement of tiltrotor configurations, distributed propulsion architectures, and novel rotorcraft technologies. As a result, the development of mechanisms aimed at suppressing whirl flutter or delaying its onset has become a critical design and research priority.

Existing research highlights the effectiveness of properly designed dynamic vibration absorbers (DVAs) in mitigating various types of vibrations (Ref. 2). Nguyen (Ref. 3) worked on mitigating the torsional vibration of an accelerating or decelerating system by adding a dynamic vibration absorber. The study confirmed that with optimum parameter values for the dynamic vibration absorber, stability can be achieved. Tehrani (Ref. 4) investigated the efficiency of the dynamic vibration absorbers attached both to the disk and to the tips of the blades. The researcher aimed to attenuate the destabilizing influence of disk eccentricity forces and improve the overall dynamic stability of the rotor system. Another study investigated various sample multi-degree-of-freedom systems, both with and without optimally designed dynamic vibration absorbers, and the numerical results demonstrated that torsional vibrations could be effectively suppressed (Ref. 5). Habib (Ref. 11) worked on integrating nonlinear tuned vibration absorbers into self-excitation mechanisms. The results of this study indicate that the inclusion of a dynamic vibration absorber leads to improved system stability.

Apart from the rotating systems, auxiliary vibration absorber configurations have also been employed in fixed-wing aircraft to provide flutter suppression, with numerical analyses confirming their efficacy. An experimental and mathematical study was conducted on an aircraft wing model with an integrated passive dynamic vibration absorber. Results showed that adding a dynamic vibration absorber increased flutter speed by 36 per cent (Ref. 8). Furthermore, Refs. 9 and 10 focused on flutter suppression by developing a wing model incorporating an active dynamic vibration absorber instead of a passive dynamic vibration absorber. The numerical results show that airfoil flutter boundaries increase with the dynamic vibration absorber addition. A similar approach was used in a two-degree-of-freedom airfoil model using nonlinear passive vibration instead of an active vibration absorber (Ref. 12). The results indicated that the flutter velocity theoretically increased. Additionally, the effect of multiple distributed passive dynamic vibration absorbers on a fixed-wing model was investigated in Ref. 13 and distributed dynamic vibration absorbers have been shown to substantially enhance flutter speed and attenuate the amplitude of limit cycle oscillations (LCOs). In Ref. 14, flutter analysis was studied by integrating a vibration absorber into a three-dimensional panel instead of a wing.

An innovative approach similar to this study was conducted in Ref. 15. The researchers used a mass spring damper model coupled to a 2-DOF rotor system to observe whirl flutter. In contrast to the present study, the overall system was observed as 3-DOF, and nonlinear spring and linear damper systems were used. Nonlinear behaviors were observed in this case, and the dynamic vibration absorber contributed positively to the operating range.

Numerous studies have been conducted on damping rotor systems using dynamic vibration absorbers and on analyzing aeroelastic stability with dynamic vibration absorbers on fixed wings. However, there is limited research on the use of dynamic vibration absorbers to mitigate whirl flutter in rotor systems. Present study explores the suppression of whirl flutter by integrating a mass-damper-spring system, which functions as a dynamic vibration absorber, into the 2-DOF rotor-nacelle system. The novelty of this approach lies in the placement of the mass within the hub of the rotor-nacelle system. A numerical whirl flutter analysis is performed using the 2-DOF Reed's model (Ref. 1), characterizing the system's dynamics through coupled pitching and yawing motions. The original model is modified to include the passive dynamic vibration absorber, and the equations of motion for the enhanced system are derived. To maintain consistency, parameters such as mass ratio and frequency ratio for the dynamic vibration absorber were tested. Whirl flutter stability is then evaluated by computing the modal damping ratios. Concisely, the study aims to demonstrate the effectiveness of passive dynamic vibration absorbers in mitigating whirl flutter, thereby contributing to the advancement of aeroelastic stability research in rotary-wing aircraft.

This paper initially introduces the classical 2-DOF whirl flutter modified model with a dynamic vibration absorber. Then, it describes the standard eigenvalue solution employed in the numerical analysis and outlines the baseline system that used for the comparison. Subsequently, it discusses key parameters to be considered when applying dynamic vibration absorbers. Finally, the numerical analysis results and corresponding comparisons are presented.

DYNAMIC MODELING

Aeromechanical Model

The 2-DOF aeromechanical model, known as Reed's model (Ref. 1), consists of a rotor supported horizontally by a pylon, which is pivoted at the wing attachment point and generates aerodynamic and gyroscopic forces, as shown in Figure 1. The propeller's spin axis is generally aligned with the free-stream flight velocity V, with minor angular fluctuations in pitch (θ) and yaw (ψ). The angular momentum of the pylon, along with the diametral moment of inertia of the rotor and the nacelle about the pivot point (I_n) and the polar moment of inertia of the rotor (I_x), is considered in the system equations of motion. The system is characterised by damping (c), stiffness (k) and rotational speed (Ω), which are used to examine the system's dynamic behaviour numerically.

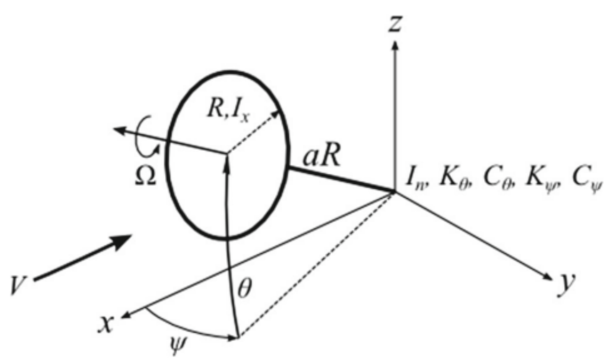

Figure 1: Whirl flutter schematic diagram (Ref. 7)

Thus, the governing equations of motion of the system can be written as follows

$$I_n\ddot{\theta}+C_\theta\dot{\theta}-I_x\Omega\dot{\psi}+K_\theta\theta=M_\theta \tag{1}$$

$$I_n\ddot{\psi}+C_\psi\dot{\psi}+I_x\Omega\dot{\theta}+K_\psi\psi=M_\psi \tag{2}$$

Where M_θ and M_ψ are the applied moments generated by aerodynamic loads in pitch and yaw, measured about the pivot point. Strip theory is used to numerically evaluate the changes and perturbations in aerodynamic loads and moments acting on the rotor blades. Eqs. 3 and 4, represent the calculated aerodynamic moments M_θ and M_ψ in a rotor system using this theory as follows (Ref. 6).

$$M_\theta=\frac{N_b}{2}K_aR\left[-(A_3+a^2A_1)\frac{\dot{\theta}}{\Omega}-A_2'\psi+aA_1'\theta\right] \tag{3}$$

$$M_\psi=\frac{N_b}{2}K_aR\left[-(A_3+a^2A_1)\frac{\dot{\psi}}{\Omega}+A_2'\theta+aA_1'\psi\right] \tag{4}$$

where N_b is the number of blades and K_a is the aerodynamic coefficient of the propeller that varies with air density, blade characteristics and rotary speed, which can be calculated by

$$K_a=\frac{1}{2}\rho c_{l,a}R^4\Omega^2 \tag{5}$$

The terms A_i are aerodynamic integrals, functions of rotor radius (R), blade chord (c) and advance ratio (μ) and can be represented, respectively, as

$$A_1=\frac{c}{R}\int_0^1\frac{\mu^2}{\sqrt{\mu^2+\eta^2}}\,d\eta \tag{6}$$

$$A_1'=\mu A_1 \tag{7}$$

$$A_2'=\frac{c}{R}\int_0^1\frac{\mu^2\eta^2}{\sqrt{\mu^2+\eta^2}}\,d\eta \tag{8}$$

$$A_3=\frac{c}{R}\int_0^1\frac{\eta^4}{\sqrt{\mu^2+\eta^2}}\,d\eta \tag{9}$$

$$\mu=\frac{V}{R\Omega} \tag{10}$$

Aeromechanical Model with Dynamic Vibration Absorber

The whirl flutter aeromechanical model is explained previously. Mathematical expressions related to the model are given in Eqs. 1 and 2, and the schematic diagram is given in Figure 1. Now, a representative model (Figure 2) is created by adding a passive dynamic vibration absorber with rotational springs and rotational dampers to this model. This dynamic system consists of four-degrees-of-freedom, with yaw and pitch motions evaluated for both the propeller and the dynamic vibration absorber. Specifically, two rotational degrees of freedom are assigned to each component, resulting in a total of four coupled dynamic variables. Since a passive dynamic vibration absorber is used, the aerodynamic forces will be taken as zero on the right side of the equations. Therefore, the system exhibits complex vibrational behavior that requires a robust and systematic approach for numerical analysis. To overcome this challenge, the standard eigenvalue solution technique is utilized.

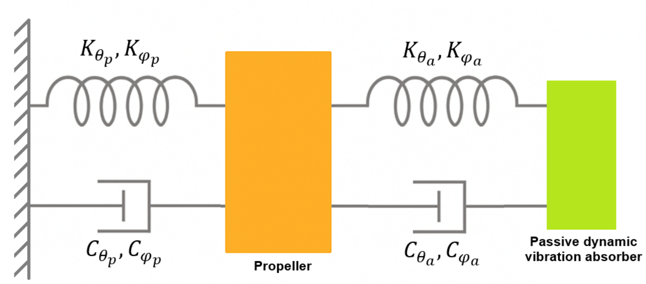

Figure 2: Representative whirl flutter model with dynamic vibration absorber.

In the modified model, the inclusion of the dynamic vibration absorber mass is expected to increase the system's stability and expand its operational speed range. The corresponding equations of motion for the updated system are given below.

$$I_{n_p}\ddot{\theta}_p + (C_{\theta_p} + C_{\theta_a})\dot{\theta}_p - C_{\theta_a}\dot{\theta}_a - I_X\Omega\dot{\psi}_p + (K_{\theta_p} + K_{\theta_a})\theta_p - K_{\theta_a}\theta_a = M_{\theta_p} \quad (11)$$

$$I_{n_p}\ddot{\psi}_p + (C_{\psi_p} + C_{\psi_a})\dot{\psi}_p - C_{\psi_a}\dot{\psi}_a + I_X\Omega\dot{\theta}_p + (K_{\psi_p} + K_{\psi_a})\psi_p - K_{\psi_a}\theta_a = M_{\psi_p} \quad (12)$$

$$I_{n_a}\ddot{\theta}_a + C_{\theta_a}\dot{\theta}_a - C_{\theta_a}\dot{\theta}_p + K_{\theta_a}\theta_a - K_{\theta_a}\theta_p = 0 \quad (13)$$

$$I_{n_a}\ddot{\psi}_a + C_{\psi_a}\dot{\psi}_a - C_{\psi_a}\dot{\psi}_p + K_{\psi_a}\psi_a - K_{\psi_a}\psi_p = 0 \quad (14)$$

Eigenvalue Solution

The moment equations can be integrated into the equations of motion of the system and obtain the system behaviours numerically by using the standard eigenvalue solution (Ref. 16). This method enables the determination of the system's dynamic response by solving the characteristic equation derived from the coupled equations of motion. Through this approach, key insights into the stability and resonance behaviors of the propeller-nacelle system and propeller-nacelle-absorber system are obtained, which are critical for both design optimization and flutter suppression strategies in rotating systems. For the modified system presented before, Eqs. 11-14 can be written in matrix form as follows:

$$\begin{bmatrix} I_{np} & 0 & 0 & 0 \\ 0 & I_{np} & 0 & 0 \\ 0 & 0 & I_{na} & 0 \\ 0 & 0 & 0 & I_{na} \end{bmatrix} \begin{Bmatrix} \ddot{\theta}_p \\ \ddot{\psi}_p \\ \ddot{\theta}_a \\ \ddot{\psi}_a \end{Bmatrix} + \begin{bmatrix} C_{\theta_p} + C_{\theta_a} & -I_X\Omega & -C_{\theta_a} & 0 \\ I_X\Omega & C_{\psi_p} + C_{\psi_a} & 0 & -C_{\psi_a} \\ -C_{\theta_p} & 0 & C_{\theta_a} & 0 \\ 0 & -C_{\psi_p} & 0 & C_{\psi_a} \end{bmatrix} \begin{Bmatrix} \dot{\theta}_p \\ \dot{\psi}_p \\ \dot{\theta}_a \\ \dot{\psi}_a \end{Bmatrix} + \begin{bmatrix} K_{\theta_p} + K_{\theta_a} & 0 & -K_{\theta_a} & 0 \\ 0 & K_{\psi_p} + K_{\psi_a} & 0 & -K_{\psi_a} \\ -K_{\theta_p} & 0 & K_{\theta_a} & 0 \\ 0 & -K_{\psi_p} & 0 & K_{\psi_a} \end{bmatrix} \begin{Bmatrix} \theta_p \\ \psi_p \\ \theta_a \\ \psi_a \end{Bmatrix} = \begin{bmatrix} M_{\theta_p} \\ M_{\psi_p} \\ 0 \\ 0 \end{bmatrix} \quad (15)$$

and this matrix form can be represented as

$$[M]\ddot{q}(t) + ([C] + \Omega[G])\dot{q}(t) + [K]q(t) = 0 \quad (16)$$

where M and G represent the mass and gyroscopic matrices, respectively, C and K are the damping and stiffness matrices that integrated aerodynamic coefficients that comes from aerodynamic moment equations (Eqs. 3 and 4). Also, $q(t)$ is the generalized coordinate for a 4-DOF system:

$$q = \begin{bmatrix} \theta_p \\ \psi_p \\ \theta_a \\ \psi_a \end{bmatrix} \quad (17)$$

To facilitate modal analysis via the standard eigenvalue approach, the governing system equations in Eq. 16 can be reformulated using an inverse matrix formulation as presented below

$$\ddot{q}(t) + M^{-1}(C + \Omega G)\dot{q}(t) + M^{-1}Kq(t) = 0 \quad (18)$$

the state space representation of the given system with the state vectors $x = \begin{Bmatrix} q \\ \dot{q} \end{Bmatrix}$ and $\dot{x} = \begin{Bmatrix} \dot{q} \\ \ddot{q} \end{Bmatrix}$ is

$$\begin{Bmatrix} \dot{q} \\ \ddot{q} \end{Bmatrix} = \begin{bmatrix} 0 & I \\ -M^{-1}K & -M^{-1}C \end{bmatrix} \begin{Bmatrix} q \\ \dot{q} \end{Bmatrix} \quad (19)$$

where I represents the identity matrix. Hence, the standard eigenvalue problem becomes

$$\dot{x} = Ax \quad (20)$$

The eigenvalues (λ_i) of the system matrix A contain critical information regarding the system's vibrational modes, specifically their natural frequencies and associated modal damping ratios, which explains the stability characteristics. The corresponding right eigenvectors characterize the mode shapes of each vibration mode. MATLAB R2025a is used for conducting eigenvalue analysis. For each mode, the undamped natural frequency ω and the damping ratio ζ are extracted from the real and imaginary parts of the complex eigenvalues, as defined in Eqs. 21 and 22.

$$\omega_i = \sqrt{Re(\lambda_i)^2 + Im(\lambda_i)^2} \quad (21)$$

$$\zeta_i = \frac{-Re(\lambda_i)}{\omega_i} \quad (22)$$

SYSTEM AND ABSORBER CHARACTERISTICS

Baseline Model

To evaluate the impact of a passive dynamic vibration absorber on whirl flutter, the system without a vibration absorber must first be analysed. Mair (Ref 7.) proposed a linearised form of the 2-DOF propeller–nacelle model to facilitate analytical investigation of the system's dynamic behavior. This baseline analysis enables a comparative evaluation of systems with and without the dynamic vibration absorber. For comparison graphs, the advance ratio, defined as the ratio of blade tip speed to forward flight speed, is taken as a variable. In calculating the advance ratio, the forward speed is held constant, allowing variations in whirl flutter speed to be analysed based on changes in blade tip speed. The key system parameters dependent on this variable are the natural frequency and modal damping ratio. From the modal damping graphs based on the advance ratio, the advance ratio value at which the damping value becomes negative is taken and the freestream velocity is calculated accordingly. The goal of this study is to increase the freestream velocity of the referenced linearised system and compare the results with the baseline system. The parameters for the baseline system are given in Table 1.

Table 1: Baseline System Parameters (Ref. 7)

Description	Symbol	Value
Rotor radius	R	0.152 m
Rotor angular velocity	Ω	40 $rads^{-1}$
Pivot length to rotor radius ratio	a	0.25
Rotor moment of inertia	I_x	0.000103 kgm^2
Nacelle and propeller moment of inertia	I_{np}	0.000178 kgm^2
Air density	ρ	1.225 kg/m^3
Blade lift slope	c_{la}	$2\pi\ rad^{-1}$
Blade chord	c	0.026 m
Number of blades	N_b	4
Propeller structural pitch damping	C_{θ_p}	0.001 $Nm\ s/rad$
Propeller structural pitch stiffness	K_{θ_p}	0.4 Nm/rad
Propeller structural yaw damping	C_{ψ_p}	0.001 $Nm\ s/rad$
Propeller structural yaw stiffness	K_{ψ_p}	0.4 Nm/rad

Dynamic Vibration Absorber Parameters

In the implementation of a dynamic vibration absorber, the mass ratio between the absorber and the primary system, along with the frequency ratio relative to the excitation frequency, are two of the key parameters that govern its effectiveness. Inmann (Ref. 17) states that the challenge of maintaining vibration absorber effectiveness under potential shifts in driving frequency can be addressed by analyzing the mass ratio. For a rotational system, mass ratio can be define as the dynamic vibration absorber inertia divided by primary system inertia (Eq. 23).

$$\varepsilon = \frac{I_{na}}{I_{np}} \tag{23}$$

In order to observe the effect of the mass ratio parameter, the original natural frequency of the primary system without the dynamic absorber (Eq. 24) and the natural frequency of the absorber integrated system before it is attached to the primary system (Eq. 25) must be explained.

$$\omega_p = \sqrt{\frac{K_p}{I_{np}}} \tag{24}$$

$$\omega_a = \sqrt{\frac{K_a}{I_{na}}} \tag{25}$$

By combining Eqs. 23, 24 and 25, the following expression is obtained:

$$\frac{K_a}{K_p} = \varepsilon \frac{\omega_a^2}{\omega_p^2} = \varepsilon \beta^2 \tag{26}$$

Where β represents the frequency ratio. These parameters are used for the explanation of how the rotor nacelle system with integrated vibration absorber behaves at certain mass ratio (ε) and frequency ratio (β) values to increase reliability. During computations, the absorber stiffness values in the pitch and yaw directions are determined using the mass ratio and the β value. Subsequently, the damping value was obtained by adopting the damping-to-stiffness ratio of the reference system.

Table 2 contains the additional values used in the numerical analysis for the system with a dynamic vibration absorber. When calculating the dynamic vibration absorber values frequency ratio (β) of 1 are used. The dynamic vibration absorber parameters presented in the following section are used to calculate stiffness, while damping was determined based on the damping-to-stiffness ratio from the baseline model. Aerodynamic moment values for the modified system are calculated according to Eqs. 3 and 4.

Table 2: Modified System Additional Parameters

Description	Symbol	Value
Mass ratio	μ	0.05
Absorber moment of inertia	I_{na}	0.000089 kgm^2
Absorber structural pitch damping	C_{θ_a}	0.00005 $Nm\ s/rad$
Absorber structural pitch stiffness	K_{θ_a}	0.02 $Nm\ s/rad$
Absorber structural yaw damping	C_{ψ_a}	0.00005 $Nm\ s/rad$
Absorber structural yaw stiffness	K_{ψ_a}	0.02 $Nm\ s/rad$

NUMERICAL ANALYSIS RESULTS

During the evaluation of the numerical analysis results, the modal damping values dependent on the advance ratio is considered. The whirl flutter speeds at which damping became negative which corresponds signaling a flutter condition are identified. To calculate the whirl flutter speed Eq. 10 is used. The aim of this study to observe and the compare the stability of aeromechanical model and modified model with a dynamic vibration absorber. The values from the reference model are used as a basis and the corresponding parameters for the modified model are subsequently derived.

Figure 3 examines the behavior of the baseline system and five different configurations under different absorber/propeller mass ratios. In theory, the addition of a dynamic vibration absorber shifts the natural frequencies of the system further apart. For that reason, if the mass ratio is too small, the combined system will not tolerate fluctuations in the driving frequency and may fail even with slight deviations. As a rule of thumb, the mass ratio is typically selected between 0.05 and 0.25, as higher values often indicate suboptimal or inefficient design (Ref. 17).

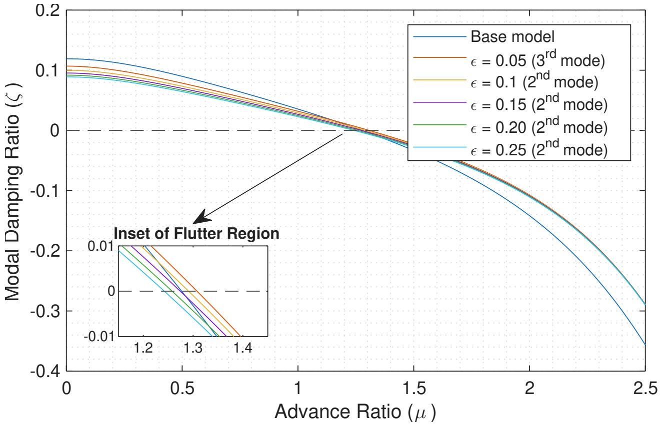

Figure 3: Modal damping ratios with different mass ratios (β = 1)

Contrary to expectations, increasing the absorber/propeller mass ratio does not consistently lead to higher operating range as seen in Figure 3. This deviation can be explained indirectly by the fact that changes in mass ratio also alter the dynamic vibration absorber's inertia, stiffness and damping characteristics, leading to mode transitions. Notably, for the system with a mass ratio of 0.5, the fluctuations start in the third mode, but for the greater mass ratios, instability begins in the second modes. From the graph based on mass ratio, when the mass ratio is 0.05 and 0.1, the whirl flutter speed increases by 6% and 2% compared to the baseline system, respectively.

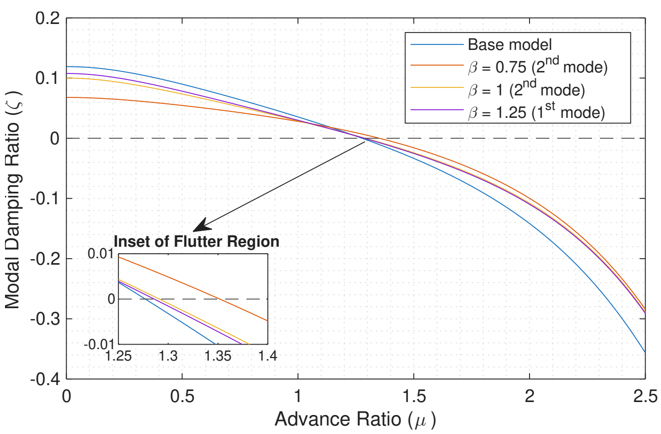

Figure 4: Modal damping ratios with different frequency ratios (μ = 0.1)

Figure 4 examines the effect of frequency ratio on modal damping-advance ratio values in systems where the absorber/propeller mass ratio value is 0.1. The frequency ratio defines the relationship between the system's excitation frequency and the natural frequency of the vibration absorber, and it is a critical parameter to ensure optimal damper performance. To evaluate how the frequency ratio influences the system's behavior when a dynamic vibration absorber is applied, numerical results are analyzed for the baseline system and for three different frequency ratio configurations. The analysis reveals that the whirl flutter speed increases when the vibration absorber's natural frequency is lower than that of the propeller. The graph indicates that when the vibration absorber frequency is set to 0.75 times the propeller's natural frequency, the whirl flutter speed increases by approximately 6% compared to the baseline system.

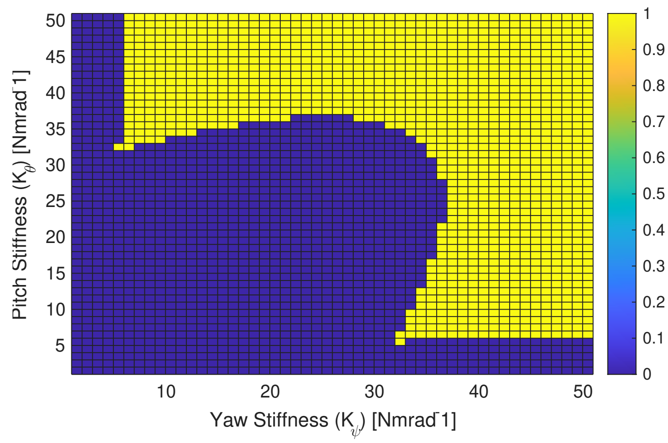

(a) Support Stiffness Stability of the Baseline System

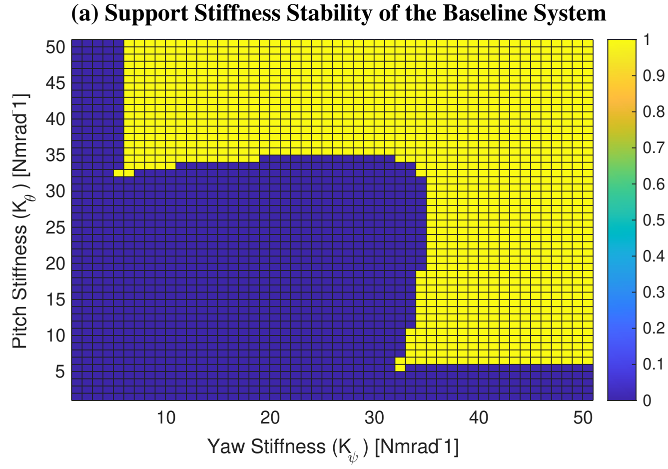

(b) Support stiffness stability of the Modified System

Figure 5: Support stiffness stability graphs for both systems

Figure 5a examines the effect of varying pitch and yaw stiffness values on the stability of the baseline system at a freestream speed of 7 m/s. Similarly, Figure 5b explores how system stability is influenced by changes in pitch and yaw stiffness for both propeller and vibration absorber, under the same freestream condition. In the graphs, the blue-shaded regions indicate that the whirl flutter speed is reached at the specified freestream velocity, while the yellow-shaded regions represent that the stability is maintained. A comparison of the two graphs shows that the yellow regions, representing stable zones, expand with the addition of the dynamic vibration absorber, indicating that the dynamic vibration absorber positively influences the system's stability.

CONCLUSIONS

The main outcomes of the study are as follows:

1. This study investigates the improvements in the stability of a propeller-nacelle model integrated with a dynamic vibration absorber.

2. The effects of both mass ratio and frequency ratio on the stability of the system with a dynamic vibration absorber are investigated.

3. It has been observed that, in systems with different mass and frequency ratios, the whirl flutter speed can increase by up to 6% compared to that of the baseline system.

Future studies should aim to analyze an optimized version of the current system by incorporating nonlinear stiffness characteristics. Moreover, identifying optimal vibration absorber parameters is expected to enhance the system's stability performance.

Author contact:
Hande Erturan erturan18@itu.edu.tr
Ali Tatar tataral@itu.edu.tr

ACKNOWLEDGMENTS

The authors gratefully acknowledge the travel support provided by Turkish Aerospace Industries for the presentation of this work. The uthors also clarify the use of large language models for grammar checking and typos.

REFERENCES

1. Reed, W. H., III, "Propeller-rotor whirl flutter: A state-of-the-art review," *Journal of Sound and Vibration*, Vol. 4, (3), 1966, pp. 526–544. DOI: 10.1016/0022-460X(66)90142-8.

2. Ormondroyd, J., and Den Hartog, J. P., "The theory of the dynamic vibration absorber," *Journal of Fluids Engineering*, Vol. 49, (2), 1928, 021007. DOI: 10.1115/1.4058553.

3. Nguyen, D. C., "Vibration control of a rotating shaft by passive mass-spring-disc dynamic vibration absorber," *Archive of mechanical engineering*, Vol. 67, (3), 2020, pp. 279–297.

4. Tehrani, G. G., and Dardel, M., "Vibration mitigation of a flexible bladed rotor dynamic system with passive dynamic absorbers," *Communications in Nonlinear Science and Numerical Simulation*, Vol. 69, 2019, pp. 1–30.

5. Vu, X. T., Nguyen, D. C., Khong, D. D., and Tong, V. C., "Closed-form solutions to the optimization of dynamic vibration absorber attached to multi-degrees-of-freedom damped linear systems under torsional excitation using the fixed-point theory," *Proceedings of the Institution of Mechanical Engineers, Part K: Journal of Multi-body Dynamics*, Vol. 232, (2), 2018, pp. 237–252.

6. Bielawa, R. L., *Rotary wing structural dynamics and aeroelasticity*, American Institute of Aeronautics and Astronautics, 2006, Chapter 11.

7. Mair, C., Rezgui, D., and Titurus, B., "Nonlinear stability analysis of whirl flutter in a rotor-nacelle system," *Nonlinear dynamics*, Vol. 94, 2018, pp. 2013–2032.

8. Verstraelen, E., Habib, G., Kerschen, G., and Dimitriadis, G., "Experimental passive flutter suppression using a linear tuned vibration absorber," *AIAA Journal*, Vol. 55, (5), 2017, pp. 1707–1722.

9. Kassem, M., Yang, Z., Gu, Y., Wang, W., and Safwat, E., "Active dynamic vibration absorber for flutter suppression," *Journal of Sound and Vibration*, Vol. 469, 2020, 115110.

10. Kassem, M., Yang, Z., Gu, Y., and Wang, W., "Modeling and control design for flutter suppression using active dynamic vibration absorber," *Journal of Vibration Engineering & Technologies*, Vol. 9, 2021, pp. 845–860.

11. Habib, G., and Kerschen, G., "Passive flutter suppression using a nonlinear tuned vibration absorber," *Nonlinear Dynamics, Volume 1: Proceedings of the 33rd IMAC, A Conference and Exposition on Structural Dynamics, Springer International Publishing*, 2016, pp. 133–144.

12. Malher, A., Touzé, C., Doaré, O., Habib, G., and Kerschen, G., "Flutter control of a two-degrees-of-freedom airfoil using a nonlinear tuned vibration absorber," *Journal of Computational and Nonlinear Dynamics*, Vol. 12, (5), 2017, 051016.

13. Basta, E., Ghommem, M., and Emam, S., "Flutter control and mitigation of limit cycle oscillations in aircraft wings using distributed vibration absorbers," *Nonlinear Dynamics*, Vol. 106, 2021, pp. 1975–2003.

14. Zhou, J., Xu, M., Yang, Z., and Gu, Y., "Suppression of panel flutter response in supersonic airflow using a nonlinear vibration absorber," *International Journal of Non-Linear Mechanics*, Vol. 133, 2021, 103714.

15. Dos Santos, J. P. T. P., Araujo G. P., and Marques, F. D., "Passive Mitigation of Whirl Flutter via Nonlinear Vibration Absorber," XX International Symposium on Dynamic Problems of Mechanics, Águas de Lindóia, Brazil, March 9-14, 2025, 2021, 103714.

16. Tatar, A., Salles, L., Haslam, A. H., and Schwingshackl, C. W., *Comparison of computational generalized and standard eigenvalue solutions of rotating systems, Topics in Modal Analysis & Testing, Volume 9: Proceedings of the 36th IMAC, A Conference and Exposition on Structural Dynamics 2018*, 2018, pp. 187-194.

17. Inman, D. J., and Singh, R. C., *Inman, D. J., & Singh, R. C.*, Englewood Cliffs, NJ: Prentice Hall, 1994, Chapter 5.